Engineering Geology 321 (2023) 107137

Contents lists available at ScienceDirect

Engineering Geology

journal homepage: www.elsevier.com/locate/enggeo

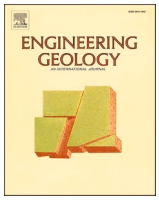

Enhanced borehole stability analysis for geological waste disposal under conditions of *in-situ* stress uncertainty: The case of Yamin Plain, Israel

Aram Yakoby [a], Yossef H. Hatzor [b], Shmulik Pinkert [a,*]

[a] Department of Civil and Environmental Engineering, Ben-Gurion University of the Negev, Beer Sheva, Israel
[b] Department of Earth and Environmental Science, Ben-Gurion University of the Negev, Beer Sheva, Israel

ARTICLE INFO

Keywords:
Borehole stability
Underground waste disposal
In-situ stress
Enhanced boundary condition

ABSTRACT

This work presents a comprehensive parametric study of unsupported and supported vertical boreholes in deep geological deposits. The parametric study is demonstrated for the case of Yamin Plain area, which is the designated site for radioactive waste disposal in Israel, where uncertainty exists regarding the *in-situ* stresses. The Yamin case is suitable for this study as the target rock layers are of marginal stability under the applied stresses, and therefore a detailed analysis is called for. A parametric factor of safety analysis is utilized for the evaluation of the borehole stability, with and without structural support. To this aim, the estimated stress field is evaluated using both analytical calculations and advanced numerical analyses, incorporating a new spring-boundary condition that yields far greater accuracy than with the commonly used boundary conditions. The parametric study for the borehole stability problem is examined with respect to the *in-situ* stresses and the structural support. We find that a steel liner is safe under any *in-situ* stress scenario; HDPE liner is found to be insensitive to liner thickness for the stress scenarios examined, because of the compatibility between the stiffnesses of the rock mass and the liner material; because of the relatively high difference between compressive and tensile strengths of concrete, we find that beyond a certain liner thickness the stability of a concrete liner in fact decreases.

1. Introduction

Radioactive waste is a byproduct of the use of radioactive materials in industries such as energy, medicine, and military. Management and disposal of radioactive waste draws increasing interest in recent decades in the context of environmental sustainability, with the goal of reducing or preventing pollution or exposure to humans. The particular waste management method used depends on the waste classification and on local authority regulations (*e.g.* IAEA, 2009). To create a uniform framework for waste management, the International Atomic Energy Agency (IAEA) published safety guides that include general descriptions and principles for the entire management process, according to the waste classification. For waste classified as High-Level Waste (HLW), the IAEA recommends burial at geological depth of at least several hundred meters below ground surface (IAEA, 2009). The option of geological storage is currently the most favored solution worldwide (Bodansky, 2004; NEA, 2008; IAEA, 2009; European Union, 2011; Birkholzer et al., 2012; Ewing et al., 2016). However, the geological storage method has not yet been implemented anywhere, because of engineering geology challenges as well as civil and political concerns (World Nuclear Association, 2021).

One of the major engineering geology challenges in deep waste disposal is to ensure the opening stability over the long-term radioactivity of the waste material. Stability of deep openings is typically studied through the fields of geomechanical and geological engineering, based on mechanical characterization of the host rock and parametrization of the subsurface deposits and the geological formations. Among these parameters are the geological structure, rock quality, stress-strain relations, the strength criterion, *etc.*, all of which influence the mechanical behavior of the host geological medium and should be determined for safe and sustainable design (Ong and Roegiers, 1993; Park and Kim, 2006; Meier et al., 2015; Kumari et al., 2017; Karimi-Khajelangi and Noorian-Bidgoli, 2022). In addition to satisfying the borehole stability, the waste disposal problem requires the consideration of other aspects such as the rock permeability, the chemical and radioactive reaction with the host sediment, the ground water table depth, and other geo-environmental parameters (Félix et al., 1996; Hudson et al., 2001; MacQuarrie and Mayer, 2005; Ewing et al., 2016; Swift and Bonano, 2016).

The engineering design of geological storage for hazardous waste in

* Corresponding author.
E-mail address: pinkerts@bgu.ac.il (S. Pinkert).

https://doi.org/10.1016/j.enggeo.2023.107137
Received 8 September 2022; Received in revised form 29 March 2023; Accepted 30 April 2023
Available online 2 May 2023

deep underground openings typically faces challenge of uncertainty particularly in the mechanical properties and in the magnitude and direction of the initial *in-situ* stresses. These uncertainties are of great concern primarily during preliminary design stages, before conducting comprehensive site investigations. For example, uncertainties in the stress ratio and the mechanical parameters of the host rock may lead to overly conservative design with taxing economic implications. Yet, such uncertainties may also lead to unsafe design, particularly when the safety limits are shown to be highly sensitive to the relationship between the strength of the material and the range of possible stress concentrations around the designed openings (*e.g.*, Shen et al., 2022). It is therefore necessary to include uncertainty and sensitivity analyses in such cases (Juang et al., 2019).

This paper presents stability analyses for waste disposal boreholes with uncertainty regarding the *in-situ* stresses and mechanical properties. We combine existing analytical solutions coupled with enhanced numerical analyses to demonstrate the sensitivity of the design to such uncertainties using the case of Yamin Plain, Israel (Dody et al., 2017; Bauer et al., 2021), as an example.

2. The special case of Yamin Plain

In this paper, the Yamin Plain area in Israel is examined, as it has been selected for a national waste disposal site, due to regulatory restrictions rather than its favorable geological conditions. The Yamin case is suitable for our study, since it is possible that some of the geological layers in the Yamin Plain would not be mechanically optimal for the borehole stability assurance, and therefore advanced analysis should be considered.

2.1. Geological setting

The Yamin Plain area is located at the Rotem syncline, which is part of the Syrian arc system of synclines and anticlines stretching from north-east to south-west (Garfunkel, 1978). Fig. 1 illustrates the geological structure in the vicinity of Yamin Plain. As shown, Rotem syncline is located between Hatire anticline and Hazera anticline, which are associated with the formations of the Yeruham Crater and the Small Crater, respectively. The figure presents the geological stratigraphy divided into five main groups; [1] Dead Sea group – consists of Hazeva sandstone formation overlying conglomerate, [2] Mount Scopus group – divided into three overlaying formations of Ghareb (chalk), Mishash (chert) and Menuha (chalk), [3] Judea group – consists of dolomites and limestones, [4] Kurnub group – mainly clays and sands, and [5] Arad group – mainly marls and limestones (Hirsch, 1995; Minster, 1996; Roded, 1996; Calvo et al., 2019). Due to estimated water table depth of ~500 m below the Yamin Plain surface, this study examines the possibility of radioactive waste disposal only at the two upper geological groups; Dead Sea and Mount Scopus. Fig. 2 describes the geological formations within these groups, at the A-A section which is delineated in Fig. 1. Note, that the Ghareb formation is divided into two subformations: Upper Ghareb and Lower Ghareb. Because of the arid climate and the low water table depth in the Yamin Plain, the disposal site can be determined to be hosted in the unsaturated zone (Calvo et al., 2019), and therefore pore water pressure effects on the mechanical properties are not considered in our analysis.

2.2. Mechanical properties

This paper describes a mechanical stability analysis for waste disposal with high-level of uncertainty in rock properties, as only a few tests were performed on selected borehole samples by commercial laboratories (in the Yamin Plain case). The representative data for engineering design relevant to our study are summarized in Table 1 which was originally compiled by Hatzor (2013) based on site investigation data reported by Levin (2013). For each geological formation, the table presents the top and bottom depths, the unit weight, γ, Young's modulus, E, Poisson ratio, ν, and the uniaxial compressive strength (UCS) which is known for only three formations. It should be pointed out that the Lower Ghareb formation, located in the middle of the examined section, is characterized by relatively low stiffness and strength values, and therefore may be problematic for engineering design.

3. Spatial stress distribution

3.1. Initial, far-field, in-situ stresses

In the absence of reliable *in-situ* stress measurements in the vicinity of Yamin Plain, we assume the principal directions of the *in-situ* stresses at the site to be the vertical (z) and two orthogonal horizontal (x and y) directions. The *in-situ* vertical stress, σ_z^i, is defined as the overburden pressure, depending on the sediment density, given by:

$$\sigma_z^i(z) = \int_0^z \gamma(\bar{z})\mathrm{d}\bar{z} \tag{1}$$

Let us define the y axis such that the *in-situ* stress in this direction is defined by the horizontal earth pressure coefficient at rest, K_0. In this work, the parameter K_0 is defined with a proportion, ζ, to the ratio derived from linear elasticity for isotropic material under uniaxial strain conditions:

$$\sigma_y^i(z) = K_0\sigma_z^i(z) = \zeta\frac{\nu}{1-\nu}\sigma_z^i(z) \tag{2}$$

The *in-situ* stress in the orthogonal horizontal axis, x, is defined by assuming possible amplifications due to horizontal tectonic stresses, through the ratio k:

$$\sigma_x^i(z) = k\sigma_y^i(z) = k\zeta\frac{\nu}{1-\nu}\sigma_z^i(z) \tag{3}$$

where here, due to the inherent uncertainty, k and ζ take any value between 0.5 and 2.0.

3.2. Post excavation stress field

The horizontal stress field developed due to the borehole excavation is defined by Kirsch (1898) solution (see for example Jaeger et al. (2007)) for a hole inside an infinite linear-elastic 2D plate. Kirsch

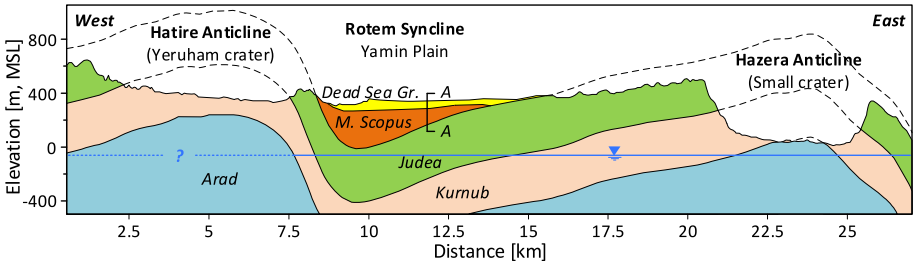

Fig. 1. East - West cross section of the geological structure in Yamin Plain. Digitized from Calvo et al. (2019).

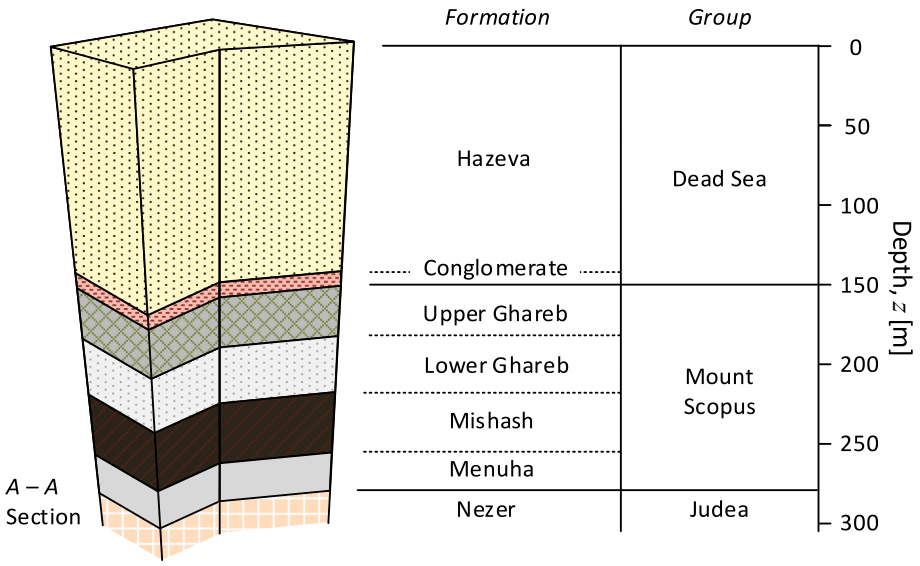

Fig. 2. Composite columnar section of the geological formations in the examined site for waste disposal in Yamin Plain.

Table 1
The available mechanical properties and estimated depths for the examined geological formations.

Formation	Depth interval [m]	γ [kN/m^3]	E [GPa]	ν	UCS [MPa]
Hazeva	0–142	20.3	1.0	0.3	–
Conglomerate	142–150	23.9	14.3	0.17	–
Upper Ghareb	150–182	21.9	9.8	0.14	10
Lower Ghareb	182–218	15.7	1.2	0.35	9.5 (187 m) 8.7 (203 m) 5.5 (215 m) 4.9 (218 m)
Mishash	218–255	19.1	4.2	0.1	–
Menuha	255–279	20.1	8.5	0.15	27
Nezer	279–300	25.5	30	0.2	–

solution considers boundary conditions of constant principal stresses at infinite distance from the hole and stress-free conditions at the hole surface. The adaptation of Kirsch solution to the current borehole problem is given by:

$$\sigma_r(z,\theta,r)=\frac{\sigma_y^i(z)}{2}\left[(1+k)\left(1-\frac{a^2}{r^2}\right)-(1-k)\left(1-4\frac{a^2}{r^2}+3\frac{a^4}{r^4}\right)cos2\theta\right] \tag{4a}$$

$$\sigma_\theta(z,\theta,r)=\frac{\sigma_y^i(z)}{2}\left[(1+k)\left(1+\frac{a^2}{r^2}\right)+(1-k)\left(1+3\frac{a^4}{r^4}\right)cos2\theta\right] \tag{4b}$$

$$\sigma_{r\theta}(z,\theta,r)=\frac{\sigma_y^i(z)}{2}\left[(1-k)\left(1+2\frac{a^2}{r^2}-3\frac{a^4}{r^4}\right)sin2\theta\right] \tag{4c}$$

where a is the borehole radius, r is the radial distance measured from the borehole center, and θ is the angle measured counterclockwise from the positive x direction, as illustrated in Fig. 3.

The post-excavation vertical stress at the borehole sides which is not considered in the original Kirsch solution is determined here using Zoback (2007)'s formulation for plane strain conditions:

$$\sigma_z(z,\theta,r=a)=\sigma_z^i(z)+2\nu\sigma_y^i(z)(1-k)cos(2\theta) \tag{5}$$

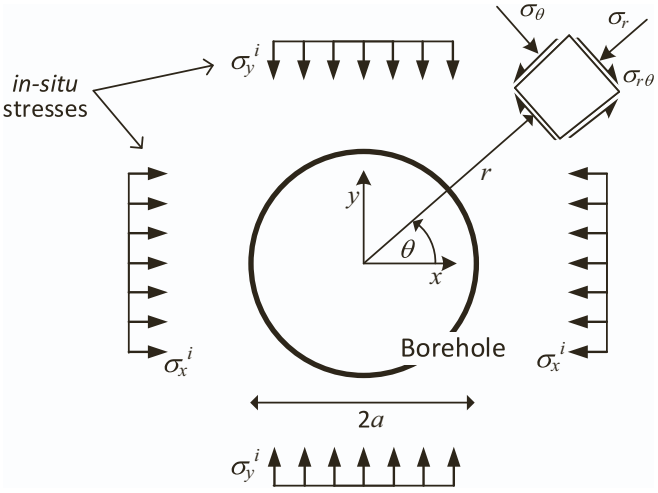

Fig. 3. Illustration of the coordinate system and sign convention of the problem.

where here pore pressures are ignored since the site is located above the ground water table. At the borehole sides ($r = a$), $\sigma_r = \sigma_{r\theta} = 0$ and therefore the principal stress directions coincide with the cylindrical coordinates system. In addition, when $r = a$, both σ_θ and σ_z reach maximum values, depending on k and θ. In the case of $k = 1$ (*i.e.* uniform horizontal compression), σ_θ and σ_z are independent of θ at the borehole circumference, and $\sigma_z = \sigma_z^i$. For $k < 1$, σ_θ and σ_z reach maximum values at $\theta = 0, 180^\circ$ and minimum values at $\theta = 90, 270^\circ$. For $k > 1$, σ_θ and σ_z reach maximum values at $\theta = 90, 270^\circ$ and minimum values at $\theta = 0, 180^\circ$ (*i.e.*, the opposite trend). Let us therefore define the maximum stresses at the borehole sides, for the entire θ range, as:

$$\sigma_{\theta,max}(z)=\max_{\forall\theta}\sigma_\theta(z,\theta,r=a) \tag{6a}$$

$$\sigma_{z,max}(z)=\max_{\forall\theta}\sigma_z(z,\theta,r=a) \tag{6b}$$

Fig. 4 shows plots of $\sigma_{\theta,max}$ and $\sigma_{z,max}$ for three k values; 0.5, 1 and 2, under $\zeta = 1$. The dramatic change in the maximum stress among the different layers is due to the sharp change in ν (with an exception of $\sigma_{z,max}$ under $k = 1$) between the layers. However, practically, the vertical stress at the layers' interfaces varies smoothly, ensuring vertical

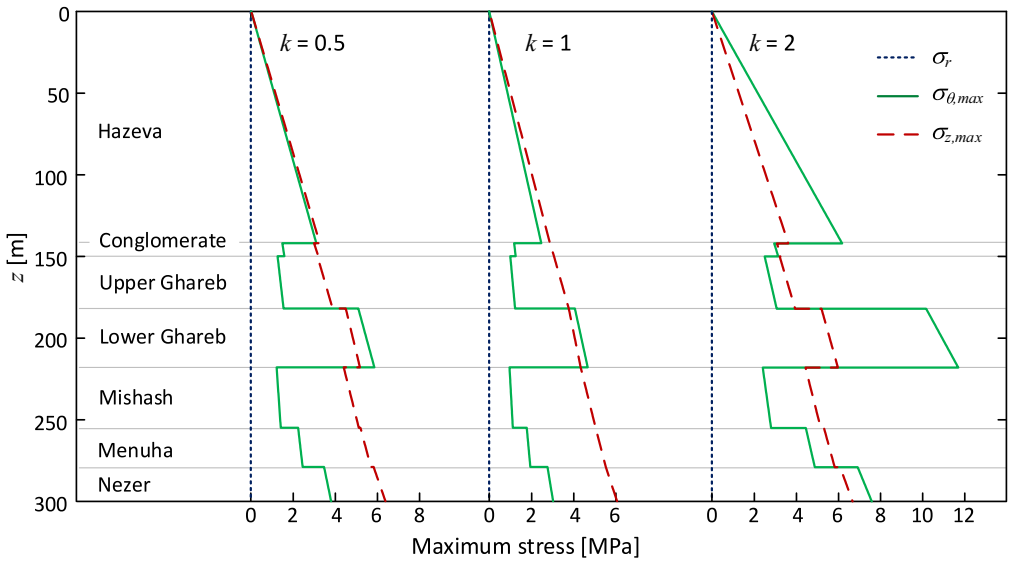

Fig. 4. Vertical profiles of the maximum stress at the borehole sides ($r = a$), for $\zeta = 1$.

equilibrium. One can also examine the minimal stresses along the borehole sides, $\sigma_{\theta,min}$ and $\sigma_{z,min}$, located at $\theta \pm 90^{\circ}$ to maximum stresses. Note that for the extreme cases of $k < 1/3$ or $k > 3$, $\sigma_{\theta,min}$ and $\sigma_{z,min}$ obtain negative values, which means that tensile stresses are developed at the borehole circumferential.

4. Factor of safety

The post-excavation stress field presented above is associated with linear elasticity solution without considering the rock strength limitations. In this work, the rock strength is determined based on Uniaxial Compressive Strength (UCS) test results. The UCS is assumed to limit the borehole sides strength, where a stress-free boundary condition exists ($\sigma_r = 0$). This work considers a failure criterion based on the maximum allowable deviatoric stress without consideration of the intermediate stress. This is due to the fact that at present only the magnitude of the unconfined compressive strength of the rock is known. Once more information is obtained regarding the mechanical behavior of this rock, a more general failure criterion that does consider the intermediate stress will be employed. Let us define a factor of safety criterion (FS) that expresses the proximity to failure at the borehole sides, given by:

$$FS = \min_{\forall\theta}\left\{\frac{UCS}{\sigma_\theta - \sigma_r}, \frac{UCS}{\sigma_z - \sigma_r}\right\} \tag{7}$$

where FS > 1 corresponds to a safe stress state, FS $= 1$ refers to a limit-equilibrium state, and FS < 1 corresponds to a theoretical failure at which the elastic solution (Eqs. 4–6; Fig. 4) exceeds the allowable stress state and therefore another, elastoplastic, solution is required. Because UCS data are available only for the Upper and Lower Ghareb and for the Menuha formations, the factor-of-safety analysis for the Yamin Plain problem is conducted here only for these formations.

The UCS distribution with depth is shown in Fig. 5a according to the geometrical and material properties presented in Table 1, accounting for linear extrapolation for the Lower Ghareb data. The UCS distribution is utilized to evaluate the variation in FS with depth (Eq. 7), illustrated in Fig. 5b for $\zeta = 1$ and three k values; 0.5, 1 and 2. In Upper Ghareb and Menuha formations, the UCS is assumed constant while the maximum deviatoric stress increases with depth, yielding a monotonic decrease in

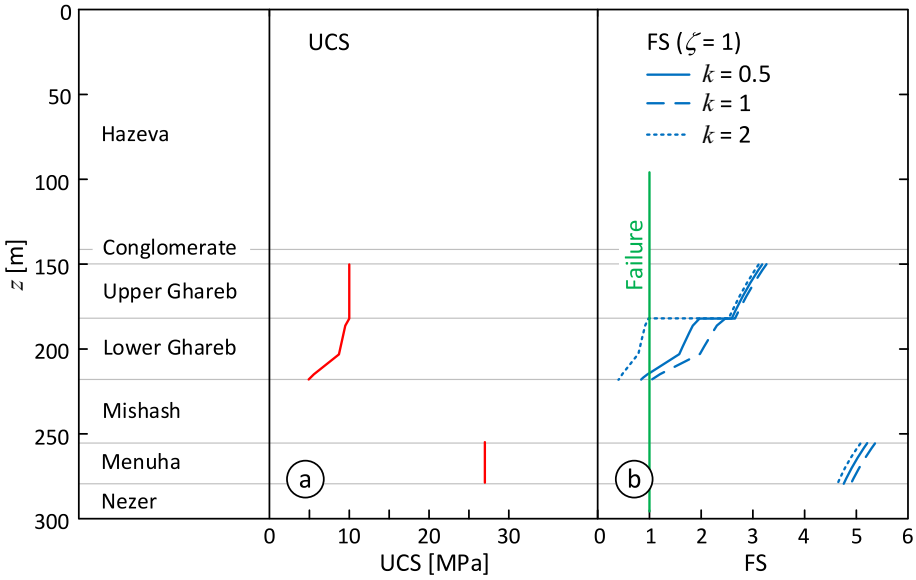

Fig. 5. (a) UCS profile with depth, and (b) FS results evaluated for $\zeta = 1$ and $k = 0.5$, 1 and 2.

FS with depth. In the Lower Ghareb, the UCS decreases with depth together with a linear increase in the deviatoric stress, yielding a steeper decrease in FS with depth. Therefore, the bottom of each examined formation can be defined as the critical depth for the borehole stability design. As can be seen from the figure, the FS values in Upper Ghareb and Menuha formations are within the range of 2.5–3.3 and 4.6–5.4, respectively, for the examined k values, which therefore can be considered safe. For the Lower Ghareb however, the three examined k values are associated with different stability scenarios. For $k = 1$, although the top layer is safe (FS = 2.5), the bottom layer is close to a failure state (FS = 1.05) which is insufficient for engineering design. In the case of $k = 0.5$ the bottom layer is in a potential failure (FS < 1), and for $k = 2$ the whole layer is potentially unstable (FS < 1).

Fig. 6 shows the dependency of FS with the parameters k and ζ, for the two examined critical depths; at the bottom of the two Ghareb units. Note that while the Upper Ghareb may be considered stable for the entire examined k and ζ ranges, in the extreme case of $k = \zeta = 2$ the FS is dramatically lower (FS = 1.63). The Lower Ghareb formation is in potential failure for most of the examined k and ζ ranges, although an unsatisfactory stability exists for $\zeta = 0.5$. In both layers, the maximum FS values are obtained for the case of horizontal uniform compression ($k = 1$) regardless of ζ values, and FS monotonically reduces with the increase of the difference between the far-field stresses. In addition, a clear trend of FS decrease is shown for greater ζ values (except for the case of $k = 1$ in the Upper Ghareb, at which $\sigma_z > \sigma_\theta$; see Eq. 7). The sudden change in FS variation at $k = 1$ is because FS is evaluated at different borehole locations ($\theta = 0°$ for $k < 1$ and $\theta = 90°$ for $k > 1$, as shown in the figure). Other abrupt changes in FS are marked in the figure, at which the major principal stress is altered (affecting the binary selection in Eq. 7).

5. The failure probability

Fig. 6 describe FS as depending on two unknown independent parameters, ζ and k, in addition to other known parameters, such as UCS, E, ν and γ. Let us therefore describe FS at a given depth depending on the two unknown parameters:

$$FS(\zeta, k) \tag{8}$$

Although ζ and k are unknown, an engineering estimation can be postulated regarding their most likely values (MLV) for the examined site, ζ_{MLV} and k_{MLV}, for which a most likely FS can be evaluated, FS_{MLV}:

$$FS_{MLV} = FS(\zeta_{MLV}, k_{MLV}) \tag{9}$$

In addition to the most likely values, one should estimate the statistical standard deviation (SD) of the unknown parameters, SD_ζ and SD_k, based on reasonable assumptions (corresponding to accumulated knowledge). Based on these estimated parameters, the statistical deviation of FS can be evaluated. A first order approximation of the standard deviation of FS, as a function of independent ζ and k, is given by (Harr, 1996):

$$SD_{FS} = \sqrt{\left(\left.\frac{\partial FS}{\partial \zeta}\right|_{\substack{\zeta=\zeta_{MLV}\\ k=k_{MLV}}}\right)^2 SD_\zeta^2 + \left(\left.\frac{\partial FS}{\partial k}\right|_{\substack{\zeta=\zeta_{MLV}\\ k=k_{MLV}}}\right)^2 SD_k^2} \tag{10}$$

Note that for specific non-differential FS neighborhood (such as the sudden change in FS shown in Fig. 6), one can use numerical approximations. Based on FS_{MLV} and SD_{FS}, a normal distribution of FS is given by:

$$f(FS) = \frac{1}{SD_{FS}\sqrt{2\pi}} exp\left[-\left(\frac{FS - FS_{MLV}}{\sqrt{2}\,SD_{FS}}\right)^2\right] \tag{11}$$

Owing to the fact that FS ≤ 1 represents a failure state, the probability to failure, P, is therefore given by:

$$P = P(FS \le 1) = \int_{-\infty}^{1} f(FS)dFS \tag{12}$$

For the Yamin Plain problem, let us consider the values ζ_{MLV}, k_{MLV},

Table 2
The assumed MLV and SD values for ζ and k, together with the calculated values of FS_{MLV}, FS_{SD} and P, for the Lower and Upper Ghareb bottoms.

Formation	ζ_{MLV}	SD_ζ	k_{MLV}	SD_k	FS_{MLV}	SD_{FS}	P [%]
Upper Ghareb	1	0.2	1.25	0.25	2.62	0.03	≈0
Lower Ghareb					0.76	0.26	82

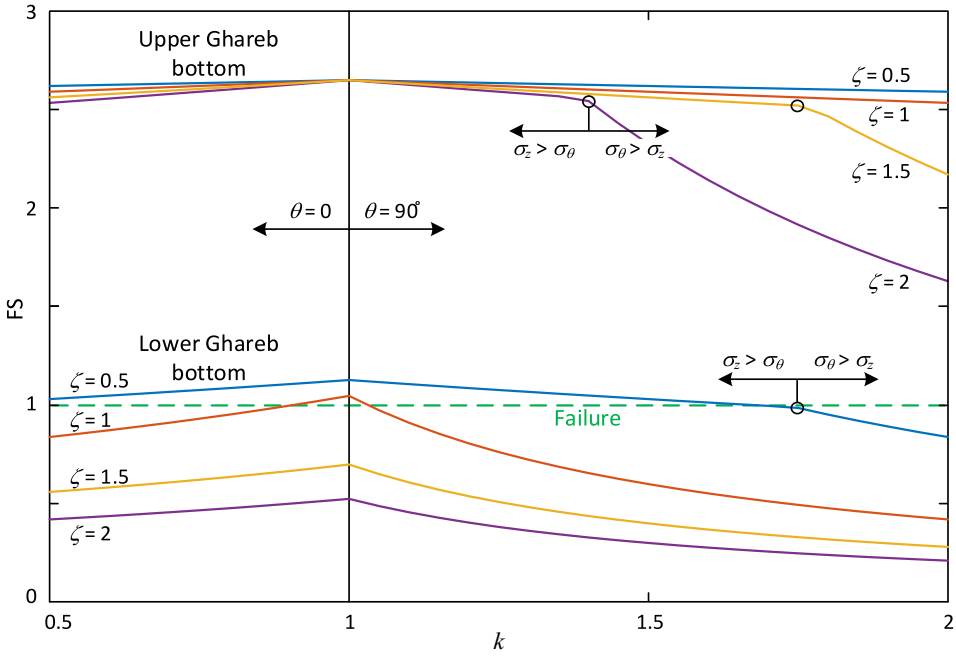

Fig. 6. FS values for the critical depths of Upper and Lower Ghareb formations, as a function of k and ζ.

SD_ζ and SD_k for both Ghareb units as given in Table 2. According to the most likely parameters, FS_{MLV} is determined as shown Fig. 6, by 0.76 and 2.62 for Lower and Upper Ghareb, respectively. Table 2 shows FS_{MLV} together with the SD_{FS} values evaluated for both Ghareb layers (Eq. 10). Fig. 7 describes the obtained normal distributions of FS for both layers. As can be seen, in the Upper Ghareb, $FS_{MLV} = 2.62$ with a narrow distribution of $SD_{FS} = 0.03$, which is clearly apparent to be stable (FS >> 1) with extremely low failure probability. In the Lower Ghareb, $FS_{MLV} = 0.76$ with a wide FS distribution of $SD_{FS} = 0.26$. The filled area in the figure is evaluated by 82% (Eq. 12), which is the probability to failure of the Lower Ghareb bottom.

6. Numerical analysis

The post-excavation stress field shown above exceeds the rock strength limit at certain depths. The calculated stress field (Eq. 4) at these depths is therefore considered invalid as it is established based on linear elasticity principles. To account for the elastoplastic rock behavior, the finite difference code FLAC^{2D} (Itasca Consulting Group, 2016) is utilized.

Fig. 8 shows the numerical grid generation for the circular opening problem, with finer grid resolution near the borehole. The numerical zones are initialized by the pre-excavation stresses (σ_x^i, σ_y^i, σ_z^i). Three boundary conditions are examined, as illustrated in Figs. 8a to 8c, respectively, as follows:

a. *Fixed boundary conditions*, in which no displacement or velocity are allowed at the grid boundaries. This boundary condition corresponds to the assumption of negligible displacements at the far-field during the borehole excavation.
b. *Stress boundary conditions*, in which the grid boundaries are constantly subjected to the initial far-field stresses (σ_x^i, σ_y^i), allowing the development of far-field displacements. This boundary condition corresponds to the assumption of negligible changes in the far-field stresses during the borehole excavation.
c. *A novel spring boundary condition*. The two aforementioned boundary conditions are built-in features in the commercial FLAC^{2D} code. In this work, an improved boundary condition is developed for enabling both displacements and stress changes at the model boundaries, that are naturally developed even in the far field. To this end, a spring boundary concept is utilized, formulated under isotropy and homogeneous material assumptions, in which the boundary displacements are associated with Kirsch (1898)'s solution (see also Jaeger et al. (2007)) while the boundary stresses are not constrained.

The boundary springs experience displacements in accordance to Kirsch (1898)'s solution, given by polar coordinates system:

$$u_r(\theta, r) = -\frac{\sigma_y^i a^2}{4Gr}\left[(1+k) - (1-k)\left(4(1-\nu) - \frac{a^2}{r^2}\right)cos2\theta\right] \quad (13)$$

$$u_\theta(\theta, r) = -\frac{\sigma_y^i a^2}{4Gr}\left[(1-k)\left(2(1-2\nu) + \frac{a^2}{r^2}\right)sin2\theta\right] \quad (14)$$

where G is the elastic shear modulus, which can be determined using E and ν (Table 1). To apply these displacements at the numerical model boundaries, the displacements are converted into Cartesian coordinates.

Fig. 9a and b show a comparison between the numerical model and the analytical solution (Kirsch, 1898) for the tangential stress distribution at the center of grid zones near the borehole circumference, $\sigma_{\theta,i=1}$, utilizing the symmetry of the solution. Fig. 9a shows $\sigma_{\theta,i=1}$ for the case of model boundaries at a distance of five diameters from the borehole center, in which a reasonable agreement with the analytical solution can be observed for the fixed-boundary and the stress-boundary conditions, while an excellent match is achieved for the newly developed spring-boundary conditions. These differences are amplified when closer boundaries are used, as can be seen in Fig. 9b for model boundaries at a distance of only one diameter from the borehole center. In this case, however, the spring boundary retains the same excellent agreement with the analytical solution. The same trend of accuracy among the three boundary conditions is presented for the radial displacements at the borehole sides, as presented in Fig. 9c and d for model boundaries located at distances of 5d and d from the borehole center, respectively. Let us define an error index for accuracy evaluation of the obtained results, given by:

$$Err_x = \left|\frac{x_{numerical} - x_{analytical}}{x_{analytical}}\right| \quad (15)$$

where x refers to the examined parameter. Table 3 presents the maximum error of $\sigma_{\theta,\ i=1}$ and u_r ($r = a$) results (Err_σ and Err_u respectively), in accordance with results shown in Fig. 9 for the three examined boundary conditions. The error values demonstrate that the spring-boundary condition improves the results accuracy by at least one order of magnitude. Besides, the agreement between the spring boundary condition and the analytical solution, regardless of the boundary location, proves the robustness of the developed boundary condition.

Among $\sigma_{\theta,\ i=1}$ variation, our main interest is in the accuracy of the maximum tangential stress at the borehole circumferential, $\sigma_{\theta,\ max}$ (Eq. 6), as it affects the determination of FS (Eq. 7). Fig. 10 shows the precision of $\sigma_{\theta,\ max}$ as a function of the boundaries location, for each of the three examined model boundary conditions. It should be noted that the

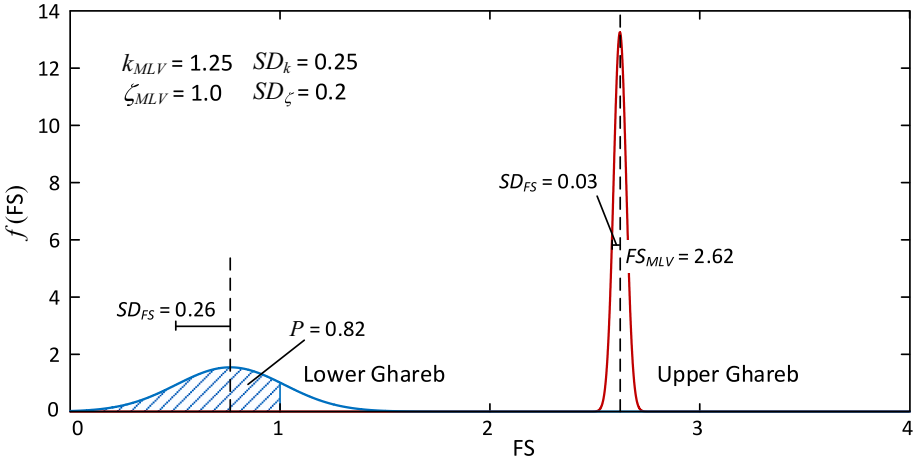

Fig. 7. Statistical distribution of FS in the critical depth of Lower and Upper Ghareb formations.

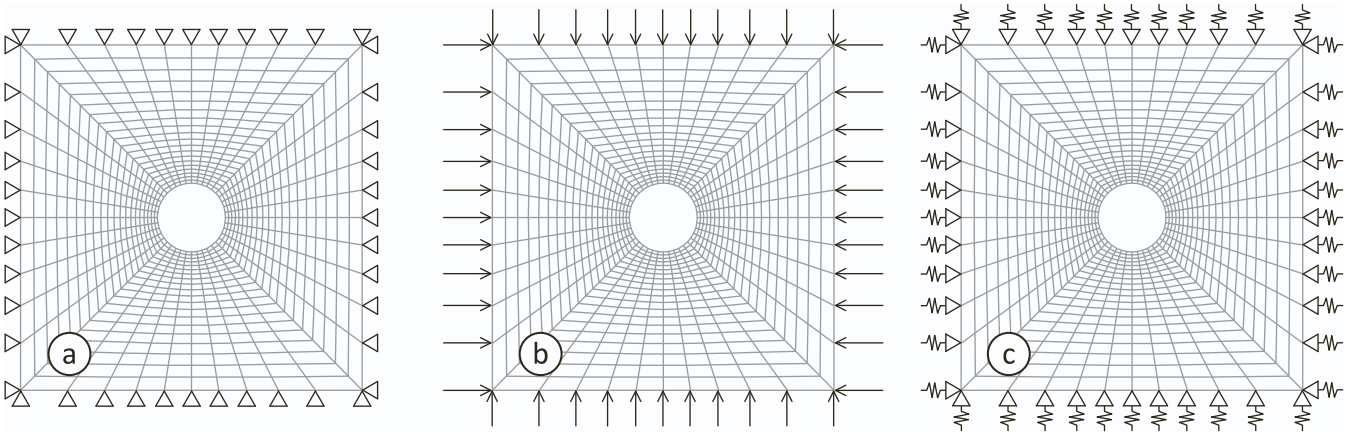

Fig. 8. Grid generation and three examined boundary conditions; (a) fixed boundary, (b) stress boundary conditions, and (c) the newly developed spring boundary. Plan view.

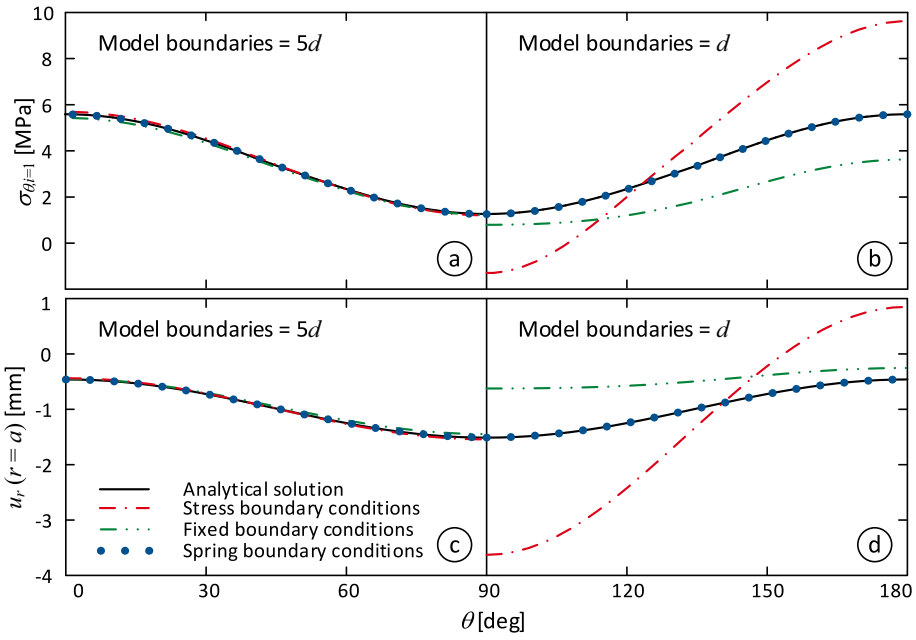

Fig. 9. Comparison of the tangential stress at the borehole sides (in the center of the grid zones at the borehole circumferential) as a function of θ, for the three examined boundary conditions, located at a distance of (a) five diameters and (b) one diameter from the borehole center, and the radial displacement at the borehole sides as a function of θ, for the same boundary conditions, located at a distance of (c) five diameters and (d) one diameter from the borehole center. Shown for $\zeta = 1$ and $k = 0.5$ at the bottom of the Lower Ghareb formation.

Table 3
Maximum relative error of $\sigma_{\theta,\ i=1}$ and $u_r(r=a)$, Err_σ and Err_u respectively, corresponding to the results shown in Fig. 9 for the three examined boundary conditions.

Boundary conditions	The maximal relative error			
	Model boundaries = 5d		Model boundaries = d	
	Err_σ	Err_u	Err_σ	Err_u
Stress boundary	4.1%	4.6%	203%	285%
Fixed boundary	3.0%	4.3%	49%	59%
Spring boundary (current study)	0.37%	0.33%	0.56%	0.20%

analytical solution and the spring boundary condition coincide, therefore the analytical solution is not plotted. As can be seen, the solutions of the three models converge in cases with far boundaries locations and diverge in solutions with model boundaries at closer distances. It is worth mentioning, that the fixed-boundary solution can be used as a lower bound and the stress-boundary solution can be used as an upper bound to the spring-boundary solution (which agrees well with the analytical solution).

As mentioned, the numerical model enables the incorporation of nonlinear stress-strain relations, accounting for both elastic and plastic material properties. In this work, the Hoek & Brown failure criterion (Hoek and Brown, 2019) is utilized, as it allows us to make use of our UCS data (Table 1) based on reasonable assumptions for continuous rocks ($a = 0.5$ and $s = 1$), and an estimated m value of 7, based on recommended value for chalks (Hoek and Brown, 1997).

Fig. 11 shows the developed plastic failure zones around the borehole, calculated for the Lower Ghareb formation. In this case, plastic failure around the opening is expected since the FS is lower than 1.0 (= 0.42; Fig. 7). Due to the potential instability at the borehole sides, the application of structural support is considered next.

7. Borehole support implementation

The implementation of structural support at the borehole sides in the FLAC^{2D} code, is performed using liner elements, which are attached to the numerical grid points at the borehole circumference. The liner thickness t (input parameter), defines the moment of inertia, I, and the cross-section area, A, per unit length of the liner element (Itasca

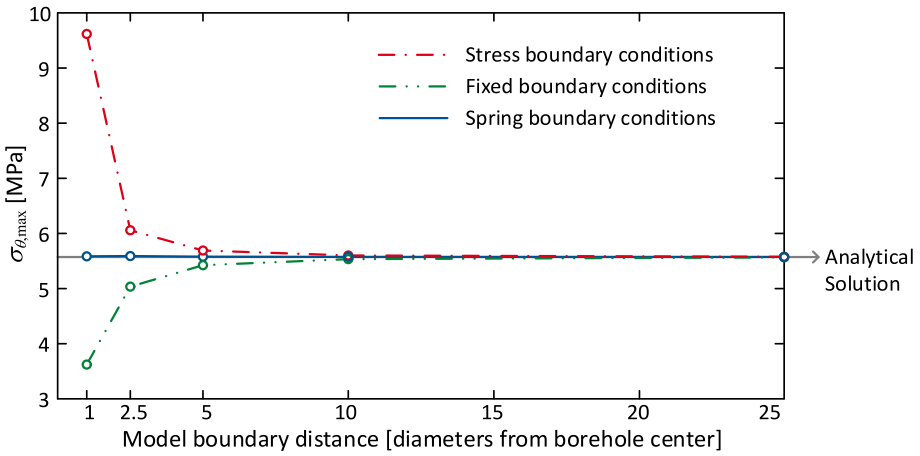

Fig. 10. $\sigma_{\theta,\ \max}$ as a function of the model boundary locations, for the three examined boundary conditions. Shown for $\zeta = 1$ and $k = 0.5$ at the bottom of the Lower Ghareb formation.

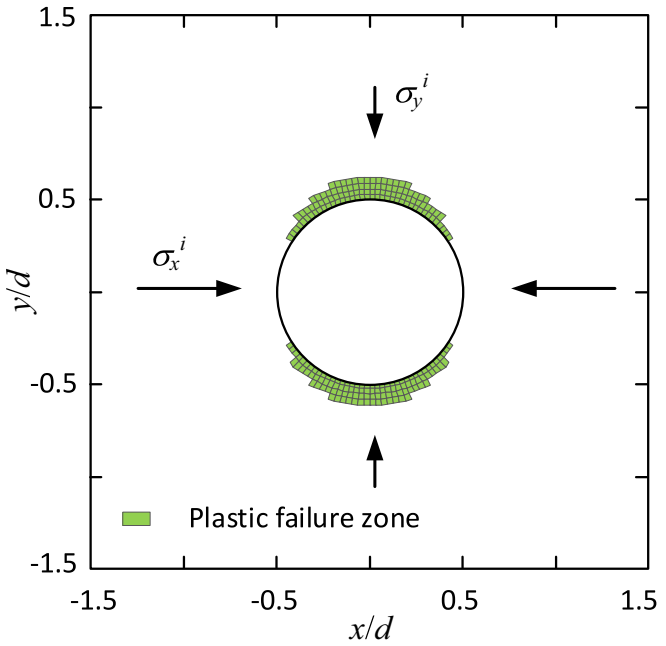

Fig. 11. Plastic failure zones around a borehole without structural support. Calculated at the bottom of the Lower Ghareb formation, accounting the Hoek & Brown plasticity model, for $\zeta = 1$ and $k = 2$. Plan view.

Consulting Group, I, 2016). Let us consider a constant net borehole diameter, D_n, which is dictated by waste disposal industry requirements. Accordingly, the numerical grid (representing the rock medium) is generated for circular borehole with a diameter of $D_n + 2\ t$. The model was verified by comparison with the analytical solution of Einstein and Schwartz (1979) which was developed for a perfectly elastic material.

We examine three different types of liner materials for the structural support; concrete, steel and high-density polyethylene (HDPE). The mechanical properties selected for the materials are described in Table 4. Note, that the concrete strength under compression is much greater than the concrete tensile strength. In addition, the stiffness of HDPE, as scaled by its Young's modulus, is very low – similar to the stiffness of the intact rock material comprising the Lower Ghareb formation.

Table 4
The mechanical properties of the three examined material types considered for structural support.

Support material	E [GPa]	ν	Compression strength, σ_{cs} [MPa]	Tensile strength, σ_{ts} [MPa]
Concrete	31.4	0.2	40	1.94
Steel	205	0.3	235	235
HDPE	1.0	0.45	8	8

In general, a nonuniform normal compression force may be developed along the structural support in case of non-uniform horizontal stresses ($k \neq 1$). In this case, the structural element also experiences bending moments. Fig. 12a and b show diagrams of normal force and bending moment distributions for the case of concrete liner of 10 cm thickness, at the bottom of Lower Ghareb formation (the same loading condition as for Fig. 11; $\zeta = 1$ and $k = 2$). In this work, the safety factor for the liner stability is examined in relation to its normal stress capacity. To this aim, let us examine the critical normal stress values developed within a cross-section of the structural support. Fig. 12c shows the variation of σ_{in} and σ_{out} along the structural support (*i.e.*, as a function of θ), associated with the forces shown in Fig. 12a and b. σ_{in} and σ_{out} in the figure refer to the normal stresses at the inner and outer fibers of the structural support. Fig. 13 shows the normal stress variation, as calculated by superimposing stresses obtained from normal force, σ_n, and bending moment, σ_m, on a given cross-section, where positive and negative signs refer to compression and tension, respectively. As can be seen in Fig. 12c, either compression or tension stresses can be developed, depending on the values of the forces. Therefore, we should examine the maximum compression stress in comparison to the compressive strength, σ_{cs} (Table 4), and in cases where tension stresses are developed, they are examined in comparison with the tensile strength values, σ_{ts} (Table 4).

The factor of safety for the stability of the structural support, FS_{sup}, is defined in this study by:

$$FS_{sup} = \begin{cases} \dfrac{\sigma_{cs}}{max(\sigma_{in}, \sigma_{out})} & if\ min(\sigma_{in}, \sigma_{out}) \geq 0 \\ min\left[\dfrac{\sigma_{cs}}{max(\sigma_{in}, \sigma_{out})}, \dfrac{-\sigma_{ts}}{min(\sigma_{in}, \sigma_{out})}\right] & if\ min(\sigma_{in}, \sigma_{out}) < 0 \end{cases} \quad (16)$$

The FS_{sup} evaluation distinguishes between the case of pure compression and the case of both compression and tension stress in the support cross-section. Note that Eq. 16 refers to the extreme σ_{in} and σ_{out} values along the support circumference.

Fig. 14 shows FS_{sup} results for the three examined support materials; (a) steel, (b) HDPE, and (c) concrete, as functions of the support thickness and under various horizontal stress ratios, k. The results are related to the critical depth of the Lower Ghareb formation under $\zeta = 1$. The

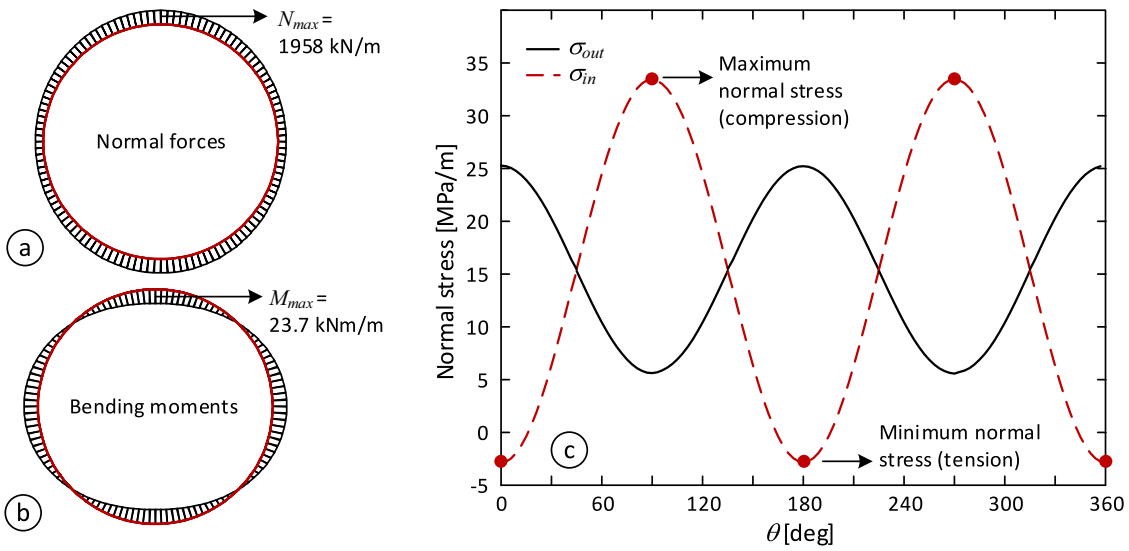

Fig. 12. (a) Normal force and (b) bending moment distributions along the structural support, associated with a 10 cm thickness of concrete support, at the bottom of Lower Ghareb formation ($\zeta = 1$ and $k = 2$), and (c) normal stresses at the inner (σ_{in}) and outer (σ_{out}) fibers variations, associated with the normal forces and bending moments in (a) and (b).

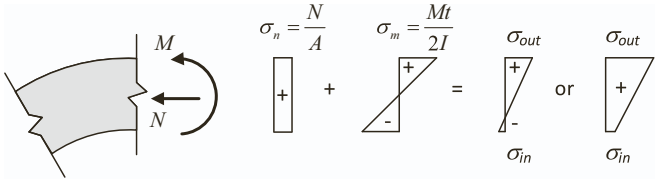

Fig. 13. Calculation scheme of normal stress distribution within the support cross-section.

filled symbols in the figure represent the factor of safety of the borehole without any support (*i.e.*, FS; Eq. 7), which were found to be usually lower than 1.0 (Fig. 6). The dashed line marks $FS_{sup} = 1$ and hence represents a failure threshold for the borehole stability. Fig. 14a shows the FS_{sup} values for the steel support, in which a borehole stability is achieved for $t \geq 1$ cm, regardless of the horizontal stress ratio in the geological formation. A monotonic increase in FS_{sup} shown with the increase in liner thickness t, such that a sufficiently high FS_{sup} is achieved for thin support thickness (for example, $FS_{sup} > 2$ when $t > 2$ cm). In addition, one should note that uniform horizontal stress ($k = 1$) is associated with the greatest FS_{sup} values, as bending moments are not developed in the structural support in this case. Fig. 14b shows the results for the HDPE, where it should be noted that the FS_{sup} results for HDPE are much lower than for the steel support, because of the significant lower HDPE strength (Table 4). Although a monotonic increase with liner thickness t is shown, FS_{sup} values for HDPE are barely sensitive to the variation in t, due to the fact that the elastic properties of the HDPE support are similar in magnitude to the rock elastic properties. Because of this insensitivity, HDPE is less effective from an engineering stand point for structural support, as further stability would be hardly improved by thickening the support. Unlike the steel and the HDPE materials, the concrete exhibits significant different strength values in tension and compression, which dramatically affects the FS_{sup} trends, as shown in Fig. 14c. As can be seen, for cases of extreme horizontal stress ratios (*i.e.* $k = 0.5$ or 2) the FS_{sup} values decay from liner thickness t greater than ~9 cm. In case of both extreme stress ratio and great liner thickness, greater bending moments would be generated on the structural support, such that tensile stresses may develop. In this case, the calculation of FS_{sup} is also influenced by the tensile strength, in addition to the compressive strength. These results show that greater liner thickness is not necessarily related to an improved borehole stability.

8. Discussion

This work presents a parametric study of a borehole stability analysis. To this aim, an example of waste disposal in the Yamin Plain of Southern Israel is examined, focusing on *in-situ* stress uncertainties. The uncertainty effect has been considered using two stress ratio parameters, between vertical and horizontal stresses (ζ) and between horizontal stresses in orthogonal directions (k). The analysis was first conducted for identifying critical depths at which an unsupported borehole would be unstable under reasonable stress uncertainty assumptions. One should note that if reliable *in-situ* stress measurements are available, one can validate the outcome of this work, or alternatively, reduce the uncertainty range. The uncertainty effect of k and ζ parameters on the design of structural support was examined, for the most critical depth. The case of concrete support demonstrates the importance of the parametric study, in which various engineering outcomes may be inferred from different stress ratios, as demonstrated in Table 5.

It is worth mentioning that during the analysis of the structural support (*via* FS_{sup}) the stability of the geological medium has not been discussed. However, if a local instability occurs in the rock medium adjacent to the (stable) structural support, it may affect other aspects, such as altering the rock permeability (which is crucial in radioactive waste disposal), induce slip across existing fractures or fracture of intact rock. Hence, the rock stability should be examined even if the structural support proves to be stable. Fig. 15 shows the maximum stress state (critical shear and normal stresses) at each zone in the numerical grid, in addition to the utilized Hoek & Brown failure criterion. As can be seen, for this specific case ($k = 2$ and $\zeta = 1$, with a 10 cm concrete support, at the Lower Ghareb formation), the entire rock medium is in a stable state; sufficiently far from the failure surface. It should be pointed out that the entire rock stress field is compressive. In fact, all cases of supported and unsupported boreholes examined in this study do not show tensile stresses within the rock medium. This is because k values were assumed between 0.5 and 2.0. However, in extreme stress ratios of $k < 1/3$ or $k > 3$, tensile stresses may develop in the surrounding rock mass (Eq. 4). Note, that the Hoek & Brown failure criterion (shown in Fig. 15) is used in this study in accordance with the scarcity of mechanical data, consisting of a limited number of UCS results. Other, more advanced failure criteria can be employed once more experimental data become available, for example the Mogi-Coulomb model; Al-Ajmi and Zimmerman (2006, 2009), that incorporates the mechanical effect of the

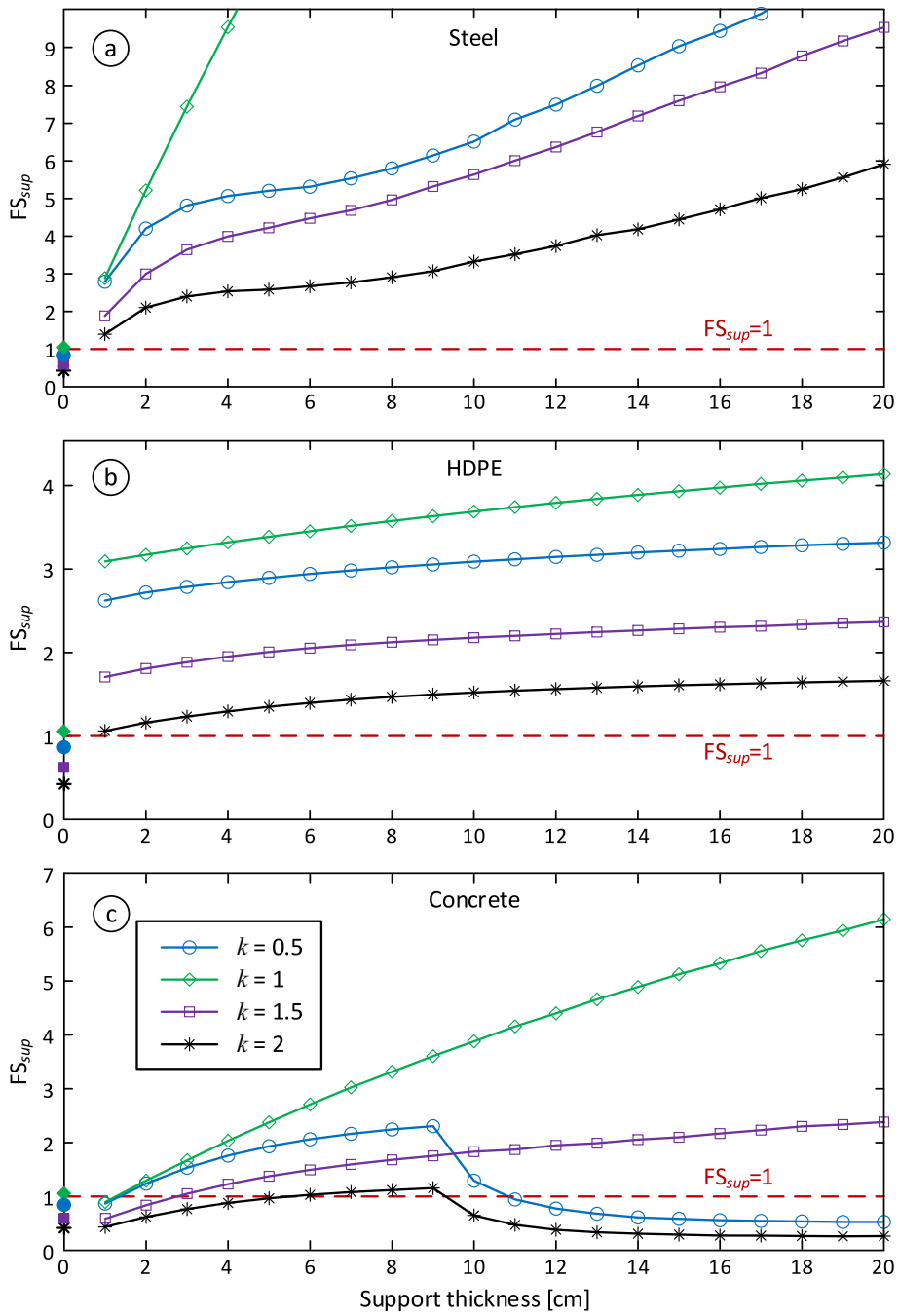

Fig. 14. FS$_{sup}$ results as function of the support thickness, for the three examined support materials; (a) steel, (b) HDPE and (c) concrete, under various horizontal stress ratios. Calculated for the critical depth of Lower Ghareb under $\zeta = 1$.

Table 5
An example of the large differences in safe concrete support thickness (FS$_{sup} > 2$) based on different *in-situ* stress assumptions. Results for $\zeta = 1$.

Requirement	k	Support thickness [cm]
FS$_{sup} > 2$	0.5	$6 \leq t \leq 9$
	1.0	$t > 4$
	1.5	$t > 14$
	2.0	no solution

intermediate stress.

The numerical model used in this study includes a novel development of a spring boundary condition. By using the newly developed spring boundaries, an excellent agreement with analytical results is demonstrated, with much better accuracy than with the default fixed or stress boundary conditions. Applying the spring boundary condition, therefore, enables utilizing models with closer boundaries to the modeled zone of interest, and improved resolutions, for better calculation efficiency. Moreover, the use of numerical grid with high resolution allows the identification of localized phenomena related to nonlinear mechanical responses. The spring boundary condition is developed based on Kirsch (1898) solution for unsupported homogeneous medium. For the case of supported borehole, the difference in stiffness between the rock and the support violates the assumptions of continuity and homogeneity employed in Kirsch solution. In this case, the boundary springs should be calibrated with an alternative model that incorporates non-homogeneity due to the structural support (*e.g.*, Einstein and

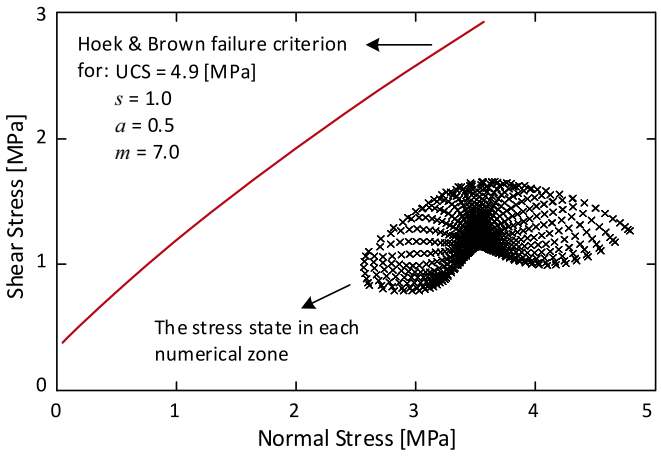

Fig. 15. The stress state at each zone in the numerical grid, together with the used Hoek and Brown failure criterion. Calculated for the Lower Ghareb formation under $k = 2$ and $\zeta = 1$, with a 10 cm concrete support.

Schwartz, 1979). We find in this study, through comparison with Einstein and Schwartz (1979) analytical solution, that the use of stress-boundary condition yields results with better accuracy in inner-forces at the structural support than when using the spring boundary. In other words, the great stiffness of the support (relative to the rock) significantly reduces stress-degradation effects at the boundary, therefore a (constant) stress-boundary condition is suitable.

The analysis of the borehole stability in this work relies on 2D calculations based on the assumption of plain strain conditions associated with an extreme borehole depth; both in the FS calculations and the horizontal cross-section analysis (*e.g.*, Fig. 11). It is recommended that further investigations should include 3D analyses, considering anisotropy and non-homogeneity effects of the subsurface (especially at the transition between overlaying rock layers).

9. Summary and conclusions

This work presents a comprehensive parametric study of stress states for vertical boreholes in deep geological deposits with and without structural support. The parametric study is demonstrated for the special case of Yamin Plain of Southern Israel that is planned to become geological radioactive waste disposal site in the future. At present there are uncertainties with respect to the *in-situ* stress conditions and therefore we examine outcomes for various theoretical stress ratios. Several important conclusions arise:

- Critical (potentially hazardous) depths can be determined using a safety factor analysis for unsupported boreholes. We find that the bottom of the Lower Ghareb formation is the critical layer, and would be unstable without application of structural support.
- All examined parametric variabilities can be integrated for engineering design by utilizing a failure probability analysis, which emphasizes the essential difference between the stability of the Lower and Upper Ghareb formations.
- A two-dimensional numerical model is presented, using a newly developed spring boundary condition that yields excellent agreement with the theoretical solution of Kirsch (1898) with respect to the mechanical behavior.
- A numerical model (FLAC^{2D}) is used to investigate the effect of the material properties of the liner used for structural support: steel, HDPE, and concrete. A safety factor analysis is conducted for structural support stability, accounting for the parametric uncertainty. We find that:
  - o Steel liner is stable under any *in-situ* stress scenario, given $\zeta = 1$.
  - o The factor of safety against failure of HDPE liner is found to be insensitive to liner thickness for the stress scenarios examined, because of the compatibility between the stiffnesses of the rock mass and the liner material.
  - o An interesting observation is found for the performance of concrete liner. Because of the relatively high difference between compressive and tensile strengths, we find that beyond a certain liner thickness the stability of the concrete liner in fact decreases.
- The stability analysis demonstrates the need for parametric study, which assists in making informed decisions even in case of parametric uncertainty with regards to such engineering geology parameters the *in-situ* stress field, the stiffness of the support materials, and the mechanical behavior of the rock mass around the borehole.

CRediT authorship contribution statement

Aram Yakoby: Conceptualization, Methodology, Software, Investigation, Formal analysis, Writing – original draft, Visualization. **Yossef H. Hatzor:** Conceptualization, Methodology, Investigation, Resources, Writing – review & editing, Supervision, Project administration, Funding acquisition. **Shmulik Pinkert:** Conceptualization, Methodology, Investigation, Resources, Writing – original draft, Writing – review & editing, Supervision, Project administration, Funding acquisition.

Declaration of Competing Interest

The authors declare that they have no known competing financial interests or personal relationships that could have appeared to influence the work reported in this paper.

Data availability

Data will be made available on request.

Acknowledgement

This research was funded by NRCN through contract # 5100029731 and by Israel Ministry of Energy through a graduate student fellowship awarded to the senior author through contract # 4501975026/220-01-022.

References

Al-Ajmi, A.M., Zimmerman, R.W., 2006. Stability analysis of vertical boreholes using the Mogi-Coulomb failure criterion. Int. J. Rock Mech. Min. Sci. 43 (8) https://doi.org/10.1016/j.ijrmms.2006.04.001.

Al-Ajmi, A.M., Zimmerman, R.W., 2009. A new well path optimization model for increased mechanical borehole stability. J. Pet. Sci. Eng. 69 (1–2) https://doi.org/10.1016/j.petrol.2009.05.018.

Bauer, S., Choens, C., Kibikas, W., Shalev, E., Lyakhovsky, V., 2021. Characterization and borehole analysis of the Ghareb Formation for nuclear waste disposal. In: 55th US Rock Mechanics/Geomechanics Symposium, ARMA 21-1662, Houston TX, June 20-23, 2021, 9 p.

Birkholzer, J., Houseworth, J., Tsang, C., 2012. Geologic disposal of high-level radioactive waste: Status, key issues, and trends. Annu. Rev. Environ. Resour. 37, 79. https://doi.org/10.1146/annurev-environ-090611-143314.

Bodansky, D., 2004. Nuclear energy. In: American Institute of Physics, 2nd ed. Springer-Verlag New York, New York. https://doi.org/10.1007/b138326.

Calvo, R., Klein-BenDavid, O., Peer, G., Sassani, D., 2019. Borehole disposal of radioactive waste in the vadose zone of the Yamin plain, Negev, Israel: Geological feasibility status report (Restricted report). In: Geological Survey of Israel, Report No. GSI/13/2019, Nuclear Research Center Negev, Report No. NRCN-ND1902, Sandia National Laboratory, Report No. SAND2019-13249 R, 54p.

Dody, A., Rosenzweig, R., Calvo, R., Shalev, E., 2017. How thick should cover layer be for radioactive waste disposal facility? The case of the Yamin plain, Israel. J. Nucl. Eng. Radiat. Sci. 3 (3) https://doi.org/10.1115/1.4035405, 030908–5.

Einstein, H.H., Schwartz, C.W., 1979. Simplified analysis for tunnel supports. J. Geotech. Eng. Div. ASCE 105 (4), 499–518.

European Union, 2011. Chemical Business NewBase – Official Journal of the European Communities L: Council Directive 2011/70/EURATOM of 19 Jul 2011 Estabilishing a Community Framework for the Responsible and Safe Management of Spent Fueland Radioactive Waste. The Financial Times Limited, Cambridge. Retrieved from: https://search.proquest.com/docview/882920502. Retrieved from:

Ewing, R.C., Whittleston, R.A., Yardley, B.W.D., 2016. Geological disposal of nuclear waste: a primer. Elements 12 (4), 233–237. https://doi.org/10.2113/gselements.12.4.233.

Félix, B., Lebon, P., Miguez, R., Plas, F., 1996. A review of the ANDRA's research programmes on the thermo-hydromechanical behavior of clay in connection with the radioactive waste disposal project in deep geological formations. Eng. Geol. 41 (1), 35–50. https://doi.org/10.1016/0013-7952(95)00025-9.

Garfunkel, Z., 1978. The Negev – regional synthesis of sedimentary basins. In: 10th International Congress on Sedimentology, Guidebook Part I: Precongress, Israel Precongress Excursion, A2, pp. 35–110.

Harr, M.E., 1996. Reliability-based design in civil engineering. Dover publications, Mineola, New York. Reprint. Originally published: New York : McGraw-Hill, 1987.

Hatzor, Y.H., 2013. Numerical simulations results using DDA method for evaluating the possible geological alternatives for radioactive waste disposal in the Yamin plane (In Hebrew). In: Unpublished Geo-Engineering Report No.8. Submitted to NNRC, November 10, 2013, 27 p.

Hirsch, F., 1995. Geological map of Israel, scale 1:50,000, sheet 19-II (Hamakhtesh Haqatan). In: The Geological Survey of Israel.

Hoek, E., Brown, E.T., 1997. Practical estimates of rock mass strength. Int. J. Rock Mech. Min. Sci. 34 (8), 1165–1186. https://doi.org/10.1016/S1365-1609(97)80069-X.

Hoek, E., Brown, E.T., 2019. The Hoek-Brown failure criterion and GSI - 2018 edition. J. Rock Mech. Geotech. Eng. 11 (3), 445–463. https://doi.org/10.1016/j.jrmge.2018.08.001.

Hudson, J.A., Stephansson, O., Andersson, J., Tsang, C., Jing, L., 2001. Coupled T–H–M issues relating to radioactive waste repository design and performance. Int. J. Rock Mech. Min. Sci. 38 (1), 143–161. https://doi.org/10.1016/S1365-1609(00)00070-8.

IAEA, 2009. International Atomic Energy Agency, Classification of radioactive waste, IAEA safety standards series no. In: GSG-1. IAEA, Vienna.

Itasca Consulting Group, I, 2016. FLAC — Fast Lagrangian Analysis of Continua, Ver. 8.0 (Computer Software). Itasca, Minneapolis, MN USA.

Jaeger, J.C., Cook, N.G.W., Zimmerman, R.W., 2007. Fundamentals of Rock Mechanics, 4th ed. Blackwell, Madlen, MA.

Juang, C.H., Zhang, J., Shen, M., Hu, J., 2019. Probabilistic methods for unified treatment of geotechnical and geological uncertainties in a geotechnical analysis. Eng. Geol. 249, 148–161. https://doi.org/10.1016/j.enggeo.2018.12.010.

Karimi-Khajelangi, B., Noorian-Bidgoli, M., 2022. Numerical study of the effect of rock anisotropy on stresses around an opening located in the fractured rock mass. J. Pet. Sci. Eng. 208, 109593 https://doi.org/10.1016/j.petrol.2021.109593.

Kirsch, G., 1898. Die theorie der elastizitat und die bedurfnisse der festigkeitslehre. Z. Ver. Dtsch. Ing. 42, 797–807.

Kumari, W.G.P., Ranjith, P.G., Perera, M.S.A., Chen, B.K., Abdulagatov, I.M., 2017. Temperature-dependent mechanical behaviour of Australian Strathbogie granite with different cooling treatments. Eng. Geol. 229, 31–44. https://doi.org/10.1016/j.enggeo.2017.09.012.

Levin, M., 2013. Y16 borehole, Final Report (In Hebrew), 21. M., Levin - Geological & Geotechnical Survey Ltd.

MacQuarrie, K.T.B., Mayer, K.U., 2005. Reactive transport modeling in fractured rock: a state-of-the-science review. Earth Sci. Rev. 72 (3), 189–227. https://doi.org/10.1016/j.earscirev.2005.07.003.

Meier, T., Rybacki, E., Backers, T., Dresen, G., 2015. Influence of bedding angle on borehole stability: a laboratory investigation of transverse isotropic oil Shale. Rock Mech. Rock. Eng. 48, 1535–1546. https://doi.org/10.1007/s00603-014-0654-1.

Minster, T., 1996. Basin Reconstruction in the Senonian Sequence, Northern Negev: A Contribution to the Understanding of Anoxic Events. In Hebrew, English abstract.

NEA, 2008. Moving Forward with Geological Disposal of Radioactive Waste A Collective Statement by the NEA Radioactive Waste Management Committee (RWMC).

Ong, S.H., Roegiers, J., 1993. Influence of anisotropies in borehole stability. Int. J. Rock Mech. Min. Sci. Geomech. Abstr. 30 (7), 1069–1075. https://doi.org/10.1016/0148-9062(93)90073-M.

Park, K., Kim, Y., 2006. Analytical solution for a circular opening in an elastic-brittle-plastic rock. Int. J. Rock Mech. Min. Sci. 43 (4), 616–622. https://doi.org/10.1016/j.ijrmms.2005.11.004.

Roded, R., 1996. Geological map of Israel, scale 1:50,000, sheet 19-I (Dimona). In: The Geological Survey of Israel.

Shen, Baotang, Shi, Jingyu, Khanal, Manoj, Mallants, Dirk, 2022. Modelling of geomechanical stability of a large-diameter, deep borehole for disposal of long-lived intermediate level waste. In: WM2022 - Waste Management 2022 Conference; 06 to end of 10 Mar 2022; Phoenix, Arizona, USA / Virtual online. WM Symposia Inc. Paper 22025. http://hdl.handle.net/102.100.100/437322?index=1.

Swift, P.N., Bonano, E.J., 2016. Geological disposal of nuclear waste in tuff: Yucca mountain (USA). Elements 12 (4), 263–268. https://doi.org/10.2113/gselements.12.4.263.

World Nuclear Association, 2021. Storage and Disposal Options: Radioactive Waste Management Appendix 2. World Nuclear Association, London. Retrieved from. https://world-nuclear.org/information-library/nuclear-fuel-cycle/nuclear-waste/storage-and-disposal-of-radioactive-waste.aspx. Retrieved from.

Zoback, M.D., 2007. Reservoir Geomechanics. Cambridge University Press, Cambridge. https://doi.org/10.1017/CBO9780511586477.